Numerical Analysis of MHD Mixed Convection and Fluid Flow in an Enclosure including a Heat Conducting Horizontal semi Circular Cylinders.

Dr. Esam M. Mohamed
Babylon Technical Institute

Abstract:

In the present work a numerical study for the effect of magneto-hydrodynamic (MHD) mixed convection flow in a vertical lid-driven square enclosure including a horizontal heat conducting semi circular cylinders on the upper and lower surfaces with Joule heating has been performed. The horizontal walls are partially insulated. The right vertical wall was maintained at uniform temperature higher than the left moving wall.

The transport equations along with appropriate boundary conditions are first transformed into non-dimensional form. The resulting non-linear system of partial differential equations are solved numerically employing the finite element formulation based on the Galerkin's method.

The computation is carried out for a wide range of relevant parameters. Parametric studies of the fluid flow and heat transfer are performed for the effects of variation of magnetic parameter (Hartmann number Ha), Joule heating parameter (J), Richardson number (Ri) and Reynolds number (Re). Results are presented for the above parameters effects on the contours of streamlines and isotherms. Besides, the heat transfer rate in terms of the local and average Nusselt number (Nu & $Nu_{av.}$) at the hot wall and average temperature of the fluid in the enclosure are offered for the mentioned parametric values. A two-dimensional laminar viscous non-compressible fluid flow was considered. The results indicated that the Hartmann number (Ha), Richardson number (Ri) and Reynolds number (Re) have strong influence on the streamlines and isotherms. On the other hand, Joule heating parameter (J) has little effect on the streamlines patterns, but a significant effect on isotherms is observed. Finally, the obtained results demonstrate that the mentioned parameters have significant effect on the local and average Nusselt number at the hot wall and the average temperature of the fluid in the enclosure. The validity of the current numerical code used is ascertained by comparing the results with previously published results under the same conditions.

الخلاصة

تم في هذا العمل انجاز دراسة عددية لتأثير الحمل الحراري المختلط الممغنط داخل حيز مربع ذو جدار عمودي أيسر متحرك ويحتوي الحيز نصف اسطوانة دائرية موصلة حراريا على كل من سطحيه العلوي والسفلي والجدران الافقية له معزولة جزئيا. تم ابقاء سطح الجدار الأيمن للحيز بدرجة حرارة منتظمة أعلى من درجة حرارة السطح المتحرك الأيسر.

تم استخدام الطريقة اللابعدية (non-dimensional form) للتعبير عن الحالات الحدودية و المعادلات الحاكمة التي تم حلها بعد تحويلها من معادلات تفاضلية إلى معادلات جبرية باستخدام طريقة (Galerkin) للعناصر المحددة (Galerkin's Finite element method).

تم إجراء الحسابات لمدى واسع من العوامل وثيقة الصلة بالموضوع. دراسة حركة المائع وانتقال الحرارة تم انجازها لتأثير تغيير معامل التمغنط (عدد هارتمن Ha) و معامل جول للتسخين (J) و عدد ريتشاردسون (Ri) وعدد رينولدز (Re). قدمت النتائج لتأثير العوامل أعلاه على كل من هيكل الجريان و توزيع درجة الحرارة بالإضافة إلى انتقال الحرارة متمثلا بعدد نسلت الكلي والموضعي عند الجدار الساخن ومعدل درجة حرارة المائع داخل الحيز, على فرض أن المائع لا انضغاطي ولزج وان الجريان طباقي ثنائي الأبعاد. بينت النتائج إن هيكل الجريان و توزيع درجة الحرارة يتأثر بمقدار كبير نتيجة تغير عدد هارتمن و كذلك عدد ريتشاردسون وعدد رينولدز, بينما كان هناك تأثير طفيف لمعامل جول للتسخين على هيكل الجريان الا أن تأثيره على توزيع درجة الحرارة يبقى ذو أهمية أيضا. وقد وجد إن العوامل المشار اليها اعلاه لها تاثير كبير ومهم على عدد نسلت الكلي و الموضعي عند الجدار الساخن, و معدل درجة حرارة المائع داخل الحيز. تم تأكيد صحة الطريقة العددية المستخدمة بمقارنة النتائج مع احد نتائج البحوث السابقة (تحت نفس الظروف).

1-Introduction:

Mixed convection in lid-driven cavities are complex problems due to shear flow caused by the movement of the moving wall and buoyancy induced flow. The influence of the magnetic field on the convective heat transfer and the mixed convection flow of the fluid are of great importance in engineering applications. A combined free and forced convection flow of an electrically conducting fluid in a cavity or in the presence of magnetic field is of special technical significance as it occur in many industrial applications such as cooling of nuclear reactors, electronic packages, micro-electronic devices, design of solar collectors, thermal design of buildings and air conditioning.

In the last several decades, there has been considerable interest in studying the influence of magnetic fields on the fluid flow dynamics and performance of various processes employing electrically conducting fluids. Some of these studies considered hydro-magnetic flows and heat transfer in many different geometries, for example, Garandet et al. (1992) [1] studied natural convection heat transfer in a rectangular enclosure with a transverse magnetic field. Rudraiah et al (1995) [2] investigated the effect of surface tension on the buoyancy driven flow of an electrically conducting fluid in a rectangular cavity in the presence of a vertical transverse magnetic field to see how this force damps hydrodynamic movements. At the same time Rudraiah et al (1995) [3] also studied the effect of magnetic field on free convection in a rectangular enclosure, they indicate that the average Nusselt number decreases with an increase in the Hartmann number and the Nusselt number approaches unity for a strong magnetic field. This shows that the convection in the enclosure is suppressed due to the introduction of the magnetic field. Khanafer and Chamkha (1998) [4] studied numerically hydro-magnetic natural convection heat transfer in an inclined square enclosure filled with a fluid saturated porous medium with heat generation. Their results indicate that the effects of magnetic field and the porous medium are found to reduce the heat transfer and fluid circulation within the cavity. Chamkha (2003) [5], made a numerical work on hydro-magnetic combined convection flow in a lid-driven cavity with internal heat generation using finite volume method. It is found that the presence of the internal heat generation leads to decreases the average Nusselt number significantly for aiding flow and to increase it for opposing flow. Kakarantzas et al. (2009) [6] studied magneto-hydrodynamic natural convection in a vertical cylindrical cavity with a sinusoidal upper wall temperature. Their results show that the increase of Rayleigh number promotes heat transfer by convection while the increase of Hartmann number favored heat conduction. Rahman et al. (2009) [7], studied the effect of a heat conducting horizontal circular cylinder positioned at the center of a lid driven enclosure on MHD mixed convection a long with joule heating. The numerical results indicated that the Hartman number, Reynolds number and Richardson number had strong effect on the streamlines, isotherms, average Nusselt number at the hot wall and average temperature of the fluid in the enclosure. Recently, Rahman et al.(2010) [8], investigated numerically, employing Galerkin weighted residual method of finite element formulation, the conjugate effect of joule heating and magnato-hydrodynamics mixed convection in an obstructed lid-driven square cavity. They showed buoyancy-induced vortex in the streamlines increases and thermal layer near the cold surface become thin and concentrated with increasing Reynolds number. Sivasakaran et al.(2011) [9], numerically studied the mixed convection in a square cavity of sinusoidal boundary temperatures at the side walls with adiabatic horizontal walls, in the presence of magnetic field. They found that the flow behavior and heat transfer rate are affected by the presence of magnetic field.

In the light of the above literature, it has been pointed out that there is no significant attention has been paid to the hydro-magnetic combined convection flow in a lid driven enclosures in presence of an obstacles like semi circular cylinders. The objective of the present study is to analyze the effect of magneto-hydrodynamic mixed convection flow in a vertical lid-driven square enclosure including a heat conducting horizontal semi circular cylinders on the upper and lower surfaces a long with joule heating using finite element method. In the current investigation, the transport phenomena will be explored by utilizing several dimensionless parameters. These parameters are the Hartmann number (Ha), Richardson number (Ri), Reynolds number (Re), Joule

heating parameter (J) and solid to fluid thermal conductivity ratio (K). The Hartmann numbers are considered from (0.0 to 40.0), Richardson number is varied from (0.0 to 10.0) to simulate forced and mixed convection dominated flow in the enclosure, while the values of Reynolds number and Joule heating parameter varied from (100 to 500) and (0.0 to 2.5) respectively. The study was achieved at constant solid to fluid thermal conductivity ratio (K=5.0) and Prandtl number (Pr=0.71). Detailed results are presented in the form of stream-lines, isotherms, local Nusselt number (Nu), average Nusselt number ($Nu_{av.}$) and average temperature in the enclosure ($\theta_{av.}$).

2- Analysis

The physical model and co-ordinate system considered in this study is illustrated in figure (1a). It is a two-dimensional square lid-driven enclosure of length (L), filled with an electrically conducting fluid with a heat conducting horizontal semi circular solid cylinders of diameter (D=0.2), placed somewhere ($L_x/2$) on the upper and lower surfaces of the enclosure. The left wall of the enclosure is allowed to move upward in its own plane at a constant velocity (U_o). Horizontal walls of the enclosure are partially insulated while the vertical walls are isothermal but the temperature of the right wall is higher than that of the left wall. The fluid is permeated by a uniform external magnetic field (B_o), the resulting convective flow is governed by the combined mechanism of driven (shear and buoyancy) force and the electromagnetic retarding force. All the physical properties of the fluid are assumed to be constant except density variation in the body force term of the momentum equation according to the Boussinesq approximation. Further, attention is focused on the effect of Hartmann number (Ha), Richardson number (Ri), Reynolds number (Re) and Joule heating parameter (J) on the flow and thermal fields as well as heat transfer of the system. Rradiation and viscous dissipation are assumed to be negligible. All solid boundaries are assumed to be rigid (i.e. no-slip walls).

2.1-Mathematical formulation

The governing equations is considered to be two-dimensional laminar, incompressible and steady state. The electrically conducting fluid is assumed to be Newtonian fluid with constant fluid properties except for the density in the buoyancy force term (i.e Boussinesq approximation). In magneto fluid mechanics, the motion of fluid is governed by the conservation equations of mass, momentum and energy. The continuity and u-momentum equations remain unchanged, but the equation of v-momentum is modified from Maxwell's field equation and Ohm's law. Also, the energy equation is modified due to the joule heating considered in the enclosure [7].

The governing equations in dimensionless form can be obtained via introducing the dimensionless variables as follows:

$X = \frac{x}{L}$, $Y = \frac{y}{L}$, $U = \frac{u}{U_o}$, $V = \frac{v}{U_o}$, $P = \frac{p}{\rho * U_o^2}$, $\theta = \frac{T - T_c}{T_h - T_c}$, $\theta_s = \frac{T_s - T_c}{T_h - T_c}$.

Based on the dimensionless variables above the governing equations (mass, momentum and energy) can be written as:

$$\frac{\partial U}{\partial X} + \frac{\partial V}{\partial Y} = 0 \qquad \text{.....(1)}$$

$$U\frac{\partial U}{\partial X} + V\frac{\partial U}{\partial Y} = -\frac{\partial P}{\partial X} + \frac{1}{Re}\left(\frac{\partial^2 U}{\partial X^2} + \frac{\partial^2 U}{\partial Y^2}\right) \qquad \text{.....(2)}$$

$$U\frac{\partial V}{\partial X} + V\frac{\partial V}{\partial Y} = -\frac{\partial P}{\partial Y} + \frac{1}{Re}\left(\frac{\partial^2 V}{\partial X^2} + \frac{\partial^2 V}{\partial Y^2}\right) + Ri\theta - \frac{Ha^2}{Re} V \qquad \text{.....(3)}$$

$$U\frac{\partial \theta}{\partial X} + V\frac{\partial \theta}{\partial Y} = \frac{1}{Re\ Pr}\left(\frac{\partial^2 \theta}{\partial X^2} + \frac{\partial^2 \theta}{\partial Y^2}\right) + J V^2 \qquad \text{.....(4)}$$

For the solid semi cylinders:

$$\frac{K}{Re\ Pr}\left(\frac{\partial^2 \theta_s}{\partial X^2} + \frac{\partial^2 \theta_s}{\partial Y^2}\right) = 0 \qquad \text{.....(5)}$$

The non-dimensional parameters in the preceding equations are the Reynolds number, Grashof number, Prandtl number, Richardson number , square of the Hartmann number, the Joule heating parameter and solid fluid thermal conductivity ratio which are defined respectively as follows:

$\mathrm{Re} = \frac{U_o * L}{\nu}$, $\mathrm{Gr} = \frac{\sigma.\beta.(T_h - T_c).L^3}{\nu^2}$, $\mathrm{Pr} = \frac{\nu}{\alpha}$, $\mathrm{Ri} = \frac{\mathrm{Gr}}{\mathrm{Re}^2}$, $\mathrm{Ha}^2 = \frac{\sigma\beta_o^2 L^2}{\mu}$, $\mathrm{J} = \frac{\sigma\beta_o^2 L U_o}{\rho C_p \Delta T}$ and $\mathrm{K} = \frac{K_s}{K_f}$.

2.2 Boundary Conditions

The dimensionless form of the boundary conditions can be written as:

$U = 0, \quad V = 1, \quad \theta = 0$ at the left vertical wall.

$U = 0, \quad V = 0, \quad \theta = 1$ at the right vertical wall.

$U = 0, \quad V = 0$ at the semi cylinders surface.

$U = 0, \quad V = 0, \quad \frac{\partial \theta}{\partial n} = 0$ at the top and bottom walls except that for the semi circular cylinders parts.

$(\frac{\partial \theta}{\partial n})_{\text{fluid}} = K(\frac{\partial \theta_s}{\partial n})_{\text{solid}}$ at the fluid-solid interface.

Where (n) is the non-dimensional distances either along X or Y direction acting normal to the surface.

2.3- Numerical Solution

The governing differential equations along with the boundary conditions has been solved by the Galerkin finite element method. The continuity equation (1) will be used as a constraint due to satisfy the mass conservation and this restriction can be used to compute the pressure distribution. To solve equations (2) - (5), the Penalty finite element method is used where the pressure P is eliminated by a penalty parameter (γ) [10]. The method under study here employ penalty schemes to handle the incompressibility condition, (div u=0). Such methods have received considerable attention in the engineering literature as it provide a manner for eliminating the pressure term from the formulation and reducing the number of unknowns [11]. So, the incompressibility criteria given by equation (1) results in:

$$P = -\gamma(\frac{\partial U}{\partial X} + \frac{\partial V}{\partial Y}) \qquad (6)$$

The continuity equation is fulfilled for large values of (γ) using equation (6) the momentum equations (2-3) become:

$$U\frac{\partial U}{\partial X} + V\frac{\partial U}{\partial Y} = \gamma\frac{\partial}{\partial X}(\frac{\partial U}{\partial X} + \frac{\partial V}{\partial Y}) + \frac{1}{\mathrm{Re}}(\frac{\partial^2 U}{\partial X^2} + \frac{\partial^2 U}{\partial Y^2}) \qquad \text{…….(7)}$$

$$U\frac{\partial V}{\partial X} + V\frac{\partial V}{\partial Y} = \gamma\frac{\partial}{\partial Y}(\frac{\partial U}{\partial X} + \frac{\partial V}{\partial Y}) + \frac{1}{\mathrm{Re}}(\frac{\partial^2 V}{\partial X^2} + \frac{\partial^2 V}{\partial Y^2}) + \mathrm{Ri}\theta - \frac{\mathrm{Ha}^2}{\mathrm{Re}} V \qquad \text{…….(8)}$$

Approximating the unknown variables, velocity (U, V) and temperature, (θ, θ_s) using basis set $\{\Phi_k\}_{k=1}^N$ as:

$$U = \sum_{k=1}^N U_k\Phi_k(X,Y),\ V = \sum_{k=1}^N V_k\Phi_k(X,Y),\ \theta = \sum_{k=1}^N \theta_k\Phi_k(X,Y) \text{ and}$$
$$\theta_s = \sum_{k=1}^N \theta_{s,k}\Phi_k(X,Y) \qquad \text{……(9)}$$

Then the Galerkin finite element method yields the following non-linear residual corresponding to the equations (4,5,7 and 8) respectively at nodes of internal domain A.

$$R_i^{(1)} = \sum_{k=1}^N \theta_k \int_A [(\sum_{k=1}^N U_k\Phi_k)\frac{\partial\Phi_k}{\partial X} + (\sum_{k=1}^N V_k\Phi_k)\frac{\partial\Phi_k}{\partial Y}]\Phi_i\, dX\, dY -$$
$$\frac{1}{Re\ Pr}\sum_{k=1}^N \theta_k \int_A [\frac{\partial\Phi_i}{\partial X}\frac{\partial\Phi_k}{\partial X} + \frac{\partial\Phi_i}{\partial Y}\frac{\partial\Phi_k}{\partial Y}]dXdY - \mathrm{J}[\int_A (\sum_{k=1}^N V_k\Phi_k)\Phi_i dXdY]^2 \quad \text{…….(10).}$$

$$R_i^{(2)} = \frac{K}{Re\ Pr}\sum_{k=1}^N \theta_{s,k} \int_A [\frac{\partial\Phi_i}{\partial X}\frac{\partial\Phi_k}{\partial X} + \frac{\partial\Phi_i}{\partial Y}\frac{\partial\Phi_k}{\partial Y}]dXdY \qquad \text{……..(11).}$$

$$R_i^{(3)} = \sum_{k=1}^{N} U_k \int_A [(\sum_{k=1}^{N} U_k \Phi_k)\frac{\partial \Phi_k}{\partial X} + (\sum_{k=1}^{N} V_k \Phi_k)\frac{\partial \Phi_k}{\partial Y}]\Phi_i \, dX \, dY -$$
$$\gamma[\sum_{k=1}^{N} U_k \int_A \frac{\partial \Phi_i}{\partial X}\frac{\partial \Phi_k}{\partial X} dXdY + \sum_{k=1}^{N} V_k \int_A \frac{\partial \Phi_i}{\partial X}\frac{\partial \Phi_k}{\partial Y} dXdY] -$$
$$\frac{1}{Re} \sum_{k=1}^{N} U_k \int_A [\frac{\partial \Phi_i}{\partial X}\frac{\partial \Phi_k}{\partial X} + \frac{\partial \Phi_i}{\partial Y}\frac{\partial \Phi_k}{\partial Y}]dXdY \quad \text{……..(12).}$$

$$R_i^{(4)} = \sum_{k=1}^{N} V_k \int_A [(\sum_{k=1}^{N} U_k \Phi_k)\frac{\partial \Phi_k}{\partial X} + (\sum_{k=1}^{N} V_k \Phi_k)\frac{\partial \Phi_k}{\partial Y}]\Phi_i \, dX \, dY -$$
$$\gamma[\sum_{k=1}^{N} U_k \int_A \frac{\partial \Phi_i}{\partial Y}\frac{\partial \Phi_k}{\partial X} dXdY + \sum_{k=1}^{N} V_k \int_A \frac{\partial \Phi_i}{\partial Y}\frac{\partial \Phi_k}{\partial Y} dXdY] -$$
$$\frac{1}{Re} \sum_{k=1}^{N} V_k \int_A [\frac{\partial \Phi_i}{\partial X}\frac{\partial \Phi_k}{\partial X} + \frac{\partial \Phi_i}{\partial Y}\frac{\partial \Phi_k}{\partial Y}]dXdY - Ri \int_A (\sum_{k=1}^{N} \theta_k \Phi_k)\Phi_i dXdY +$$
$$\frac{Ha^2}{Re} \int_A (\sum_{k=1}^{N} V_k \Phi_k)\Phi_i dXdY \quad \text{……..(13).}$$

Bi-quadratic basis functions has been used to approximate the unknown field variables and the integration done by the three point Gaussian in the residual equations. The matrix vector notation of the residuals, i.e., Equations (10)-(13) can be written as:

$$[C_1 + \gamma C_2]w = F \quad \text{…….(14)}$$

Where (w & F) denotes the unknown vector and known vector respectively, (C_1 & C_2) are the coefficient matrices obtained from the Jacobian of the residuals. The value of the penalty parameter (γ) is taken (10^8) [12] and [13]. To solve the sets of the nonlinear equations in the form of a matrix, the Newton-Raphson method has been used to solve the non-linear residual equations (10-13) and obtaining the coefficients of the expansion in equation (9). At each iteration, the linear system of equations of the order (3N × 3N):

$$J(a^n)[a^n - a^{n-1}] = R(a^n) \quad \text{…...…(15)}$$

Is solved, where (n) is the iterative index, $J(a^n)$ Jacobian matrix contains the derivatives of the residual equations and $R(a^n)$ is the vector of residuals. The iterative process is finished with the convergence criterion $\left[\sum\left(R_i^{(j)}\right)^2\right]^{0.5} \leq 10^{-5}$.

A nine node bi-quadratic elements with each element mapped using iso-parametric mapping from (X-Y) to a unit square (ξ-η) domain has been used, (see figure 1b and Appendix A) [13]. Subsequently, the domain integrals in the residual equations are obtained using nine node bi-quadratic basis functions in (ξ-η) as:

$$X = \sum_{i=1}^{9} X_i \Phi_i(\xi, \eta) \quad \text{and} \quad Y = \sum_{i=1}^{9} Y_i \Phi_i(\xi, \eta) \quad \text{……..(16) .}$$

Where $\Phi_i(\xi,\eta)$ are the local bi-quadratic basis functions on the (ξ,η) domain and (X_i ,Y_i) are the (X,Y) coordinates of the (i) nodal points, (see Appendix A). The integrals in equations (10-13) were obtained in (ξ-η) domain using the following transformation:

$$\begin{bmatrix} \frac{\partial \Phi_i}{\partial X} \\ \frac{\partial \Phi_i}{\partial Y} \end{bmatrix} = \frac{1}{J}\begin{bmatrix} \frac{\partial Y}{\partial \eta} & -\frac{\partial Y}{\partial \xi} \\ -\frac{\partial X}{\partial \eta} & \frac{\partial X}{\partial \xi} \end{bmatrix}\begin{bmatrix} \frac{\partial \Phi_i}{\partial \xi} \\ \frac{\partial \Phi_i}{\partial \eta} \end{bmatrix} \quad \text{…….(17)}$$

$$dX\,dy = J\,d\xi\,d\eta \quad \text{…….(18)}$$

$$\text{where:} \quad J = \frac{\partial (X,Y)}{\partial (\xi,\eta)} = \begin{vmatrix} \frac{\partial X}{\partial \xi} & \frac{\partial X}{\partial \eta} \\ \frac{\partial Y}{\partial \xi} & \frac{\partial Y}{\partial \eta} \end{vmatrix} \quad \text{…….(19)}$$

2.4 The stream function

The stream function (ψ) for two dimensional flows is obtained from velocity components (U and V). The relationships between stream function (ψ) and velocity components are:

$$U = \frac{\partial \psi}{\partial Y} \quad \text{and} \quad V = -\frac{\partial \psi}{\partial X} \quad \text{……..(20)}$$

Differentiate the above two relations with respect to Y and X respectively and add both sides, the following relation can be obtained:

$\frac{\partial^2 \psi}{\partial X^2} + \frac{\partial^2 \psi}{\partial Y^2} = \frac{\partial U}{\partial Y} - \frac{\partial V}{\partial X}$ ……..(21)

Approximate the stream function (ψ) using the basis function set (Φ) as $\psi = \sum_{k=1}^{N} \psi_k \Phi_k (X, Y)$ and the relation for U and V from equation (9), the Galerkin finite element method yields the following residual equation for eq. (21):

$$R_i^{(5)} = \sum_{k=1}^{N} \psi_k \int_A \left[\frac{\partial \Phi_i}{\partial X}\frac{\partial \Phi_k}{\partial X} + \frac{\partial \Phi_i}{\partial Y}\frac{\partial \Phi_k}{\partial Y}\right] dX dY + \sum_{k=1}^{N} U_k \int_A \Phi_i \frac{\partial \Phi_k}{\partial Y}\, dX\, dY -$$

$$\sum_{k=1}^{N} V_k \int_A \Phi_i \frac{\partial \Phi_k}{\partial X}\, dX\, dY \quad \text{……..(22)}$$

Since, the no slip condition is valid at all boundaries of the enclosure, hence ψ will be zero at all grid points on boundaries. The bi-quadratics basis function is used to evaluate the integrals in equation (22) and then, the stream functions are obtained by solving the (N) linear residual equation (22).

2.5 Nusselt number and average temperature

The local Nusselt number is defined by:

$Nu = -\frac{\partial \theta}{\partial n}$ ……..(23)

Where (n) denotes the normal direction on a plane. The normal derivative is obtained by the bi-quadratics basis set in (ξ-η) domain with the help of using equations (16,17 and 18). The local Nusselt number at the right side wall is defined as:

$Nu = -\sum_{i=1}^{9} \theta_i \frac{\partial \Phi_i}{\partial X}$ …….(24)

The average Nusselt number ($Nu_{av.}$) at the right side wall is:

$Nu_{av.} = \int_0^1 Nu\, dY$ ……(25)

The average temperature of the fluid in the enclosure is defined by

$(\theta_{av.} = \int \frac{\theta}{\bar{V}}\, d\bar{V})$ …….(26)

where $(\bar{V})$ is the enclosure volume.

3-Numerical Test:

The computational domain in (ξ-η) coordinates (see Appendix A) consist of 25×25 bi-quadratic elements which correspond to 51×51 grid points which are selected after performing several tests using successively sized grids, 41×41 to 81×81 to see the effect of grid size on the accuracy of results. It is seen that the bi-quadratic elements with lesser number of nodes easily capture the variations of the field variables. The computational grid in the main domain is generated by mapping the non-uniform domain elements into a square domain elements in (ξ-η) coordinate system as shown in fig. 1b and the procedure is illustrated in Appendix A. A program in Fortran language was built to find the results.

4-Numerical Code Validation:

The computational model is verified by comparison with the results of the numerical solution reported by Chamkhia [5], which is based on finite volume scheme. The results of the comparisons are listed in the table below for the average Nusselt number ($Nu_{av.}$). The comparisons show close proximity in the predictions made between the two different solutions. These validation cases ascertain the confidence in the numerical results of the present work, so it can be decided that the current code can be used to predict the flow characteristics of the present study.

The effect of (Ha) on (Nu_{av}). for Gr=100, Pr=0.71 and Re=1000.			
Parameter (Ha)	Present study-($Nu_{av.}$)	Chamkhia [5]-($Nu_{av.}$)	Error(%)
0.0	2.2071	2.2692	2.73
10.0	2.1992	2.1050	4.47
20.0	1.7171	1.6472	4.24
50.0	1.0013	0.9164	9.26

5-Results and Discussion:

The results are carried out for a steady-state mixed convection in a square enclosure with horizontal semi circular cylinders on the upper and lower surfaces. In all cases the working fluid is air, the Prandtl number has been taken as (Pr=0.71). The variation of Hartmann number (Ha), Joule heating parameter (J), Reynolds number (Re) and Richardson number (Ri) on the fluid flow and heat transfer characteristics have been studied. The results are presented in terms of streamlines and isotherm patterns. The variation of local and average Nusselt number (Nu and $Nu_{av.}$) on the hot wall, and average temperature ($\theta_{av.}$) in the enclosure are also studied.

5.1-The effect of Hartmann number

Fig. (2) depicts the effect of Hartmann number (Ha) on the flow and temperature pattern at Re=100, Ri=1.0 and J=1.0. In figs. (2) (a_1 to e_1), an intrinsic effect here is that the streamlines are interrupted by the left driven lid. It can be observed that the streamlines values decreases with increasing Hartmann number which means that the electromagnetic retarding force resulting from the magnetic field strongly affect the flow field, and there developed one vortex. The vortex with clockwise direction has developed near the left surface, since the left lid is driven from the bottom to the top. In the right part of the enclosure the streamlines are deflected downward due to effect of increasing Hartmann number despite of presence of shear and buoyancy forces which causes the vortices to rise up. The effects of Hartmann number (Ha) on the isotherms are shown in figs. 2 (a_2-e_2). From these figures it can be seen that the isotherms are concentrated near the lower half of the right vertical hot wall and become nearly parallel to its surface at that part forming a thermal boundary layer, which means that most of heat transfer process is carried out by conduction at this part. Also it can be seen that a plume starts to appear on the top side in the enclosure. The plume near the right side of the upper semi circular cylinder gradually increases forming another thermal boundary layer and near the left side gradually decreases. Generally, significant deviations of isothermal lines are observed around the semi circular cylinder that mounted at the top surface in the enclosure due to the buoyancy induced vortex.

In order to evaluate the effect of the magnetic fields on the heat transfer rate along the hot vertical right wall, local and average Nusselt number are plotted as a function of (Y) and Richardson number (Ri), respectively as shown in Fig. (3) (a & b). In Fig. (3-a), it is observed that local Nusselt number decreases with increasing of (Ha), indicating that with increasing the Hartmann number the heat transfer rate decreases.

The maximum local Nusselt number distribution occur nearly at the midpoint of the lower half of the right vertical hot wall due to high heat transfer rate at this portion, as the thermal boundary layer thickness decreases, and this is revealed by the denser concentration of isotherms near this portion as shown in figure 2 (a_2-e_2). While the local Nusselt number decreases at the upper half due to low heat transfer rate as the isotherm lines deviate away from the surface. In Fig. (3-b), it is observed that average Nusselt number increases with increasing of Richardson number (Ri) and it is always smaller for bigger values of Hartmann number (Ha).

Another evaluation is that of Fig. (3-c), which reveal that average fluid temperature in the enclosure is lower for large values of Hartmann number (Ha). It is observed that for Ha=0.0 and 10, the average temperature increases with the increase of (Ri), but for Ha=20,30 and 40 it shows an oscillatory behavior .

5.2-The effect of Joule heating parameter

Fig. 4 (a_1-e_1) and (a_2-e_2) show the distribution of the streamlines and isotherms respectively, for (J=0,1,1.5,2 &2.5) at Ri=1.0, Re=100 and Ha=10. It can be observed that the circulation of the flow in the enclosure shows one overall clockwise rotating vortex as shown in fig. 4 (a_1-e_1). For (J=0 and 1.0) the pattern of the streamlines are nearly identical and show a small downward deviation at the right part of the enclosure, while for (J=1.5, 2 and 2.5) the pattern still identical

with an increasing values of streamlines as (J) increases. Also, a careful observation indicates that the core of the vortices increases with increasing value of the Joule heating parameter (J).

Corresponding temperature distribution can be seen in figs. 4 (a_2-e_2). From these figures it can be seen that the isotherms are nearly parallel to the lower part of the vertical hot wall and start to deviate away at the upper part with increasing (J), (i.e J >1) and its distribution become more spread inside the enclosure at (J=2.5). Also we can observe that the isotherm lines near the right lower corner gradually decreases with increasing values of (J) ,as it spread away from the hot wall to affect a large area and a thick thermal boundary is seen near this corner of the enclosure for the large value of (J=2.5).

The local Nusselt number (Nu) at the vertical hot wall of the enclosure as a function of (Y) for the five different Joule heating parameters is shown in fig. 5 (a). it is shown that the local Nusselt number increases with increment of (Y) up to nearly the midpoint of the lower half of the vertical hot wall (except that for j=0.0, as it precede further), then it will steep to a lower value with increasing of (Y). This behavior is related to the distribution of isotherm lines at the vertical right wall. It is also noted that local Nusselt number is always higher for smaller Joule heating parameter (J). Another examination of fig. 5 (a) does reveal that up to (Y=0.2), local Nusselt number is lower for (J=0.0), except that for(j=2.5).

The average Nusselt number at the hot wall as a function of Richardson number (Ri) is plotted in fig. 5 (b). it is observed that for (J=0.0 and 1.0) the average Nusselt number shows a little oscillatory behavior. It is also noted that its value increases with (Ri) and is also higher for smaller Joule heating parameter (J).

Fig. 5 (c) illustrates the average temperature of the fluid in the enclosure as a function of Richardson number (Ri). It is observed that for J=0.0, the average temperature decreases with increasing of (Ri) , but for J=1.0 and 1.5 increases and for J=2.0 and 2.5 it shows a small oscillatory behavior with the increase of (Ri) and it is always high for higher Joule heating parameter (J).

5.3-The effect of Reynolds number

Fig. 6 (a_1-e_1) and (a_2-e_2) illustrates the distribution of the streamlines and isotherms for (Re=100, 200, 300, 400 and 500) at Ri=1.0, J=1.0 and Ha=10, respectively. For a small Reynolds number, (Re=100), there exists one clockwise vortex occupying the enclosure, as shown in fig. 6 (a_1). When Reynolds number increases (i.e. Re=200), a small clockwise cell
start to develop near the right vertical hot wall as shown in fig. 6 (b_1), and this cell is fully developed for bigger values of Reynolds number (i.e, Re>200), as illustrated in fig. 6 (c_1-e_1). This implies that fluid is well mixed in the enclosure at high Reynolds number. With the increasing values of Reynolds number, (Re=300, 400 and 500) the size of the clockwise cell adjacent to the right vertical hot wall gradually increases and pushing up the main clockwise vortex to the upper left corner of the enclosure and that is due to increase of shear force at the driven lid.

Corresponding temperature distributions are seen in figs. 6 (a_2-e_2), from these figures it can be seen that isothermal lines adjacent to the hot right vertical wall are nearly parallel to this wall at the lower half which is similar to conduction-like distribution. Then, isothermal lines start to turn back from the hot wall at the upper half due to the effect of the convective current. A way from the hot wall, convective distribution of the isothermal lines occurs throughout the enclosure mostly at the upper half due to the strong influence of the convective currents.

The effect of Reynolds number on the local and average Nusselt number as a function of (Y) and Richardson number (Ri), respectively, at the right hot wall for the studied values of Reynolds numbers are displayed in figure (7- a & b). From these figures, it is seen that, as we have mentioned previously, the local Nusselt number increases with (Y) up to nearly the midpoint of the lower half of the vertical hot wall, then it will steep to a lower value. The average Nusselt number is highly increases with Richardson number up to (Ri=4.0), but then it will continue with a lower rate .It is also noting that local and average Nusselt number are always upper for higher values of Reynolds number. Fig. (7-c) shows the average temperature in the enclosure as a function of Richardson number for the specified Reynolds numbers. It is observed that the average temperature for different

Reynolds number shows a higher rate of increment with increasing of Richardson number. On the other hand, the average temperature is higher for bigger values of Reynolds number.

5.4-The effect of Richardson number

The response of the streamlines and isotherms patterns to the variation of Richardson number is explained in fig. (8), for Re=100, J=1.0 and Ha=10.0. It is seen in fig. (8-a_1) that for Ri=0.0 (pure forced convection), there exists only one clockwise vortex interrupted by the driven lid, leading to a core of half an egg shape located near the centre of the left driven wall of the enclosure. From the fig. (8-b_1) it can be seen easily that for (Ri=1.0), the clockwise vortex becomes large in size and occupying the maximum part of the enclosure and its core is shifted up and away from the left driven wall due to the dominating influence of the buoyancy force. From figs. (8-c_1, d_1 and e_1) it can observe that the core of the clockwise vortex becomes wider and a small cell starts to grow slowly near the right hot wall and becomes fully developed with further increasing values of the Richardson number, which leads also to increase the strength of these eddies. These effects of Richardson number on the flow field are reasonable since increasing values of (Ri) assists buoyancy forces.

The influence of Richardson number on the isothermal lines patterns are presented in fig. 8 (a_2-e_2). From the fig. 8 (a_2) it can be seen that the isothermal lines are nearly parallel to the right vertical heated surface for Ri=0.0, whereas for further change of Ri to (1.0, 4.0, 8.0 and 10.0), it can be seen from figs. 8 (b_2- e_2) that the isothermal lines starts to deviate from the right surface on its upper part and become parabolic in shape. From these figures it can ascertain that increasing the buoyancy force as a result of increasing Richardson number, causes the isothermal lines to deform increasingly and a thermal boundary layer form near the hot surface.

5.5-Horizontal and Vertical Velocity Components at the mid section of the Enclosure:

Figures 9(a-h), display the effect of Hartmann number (Ha), Joule heating parameter (J), Reynolds number (Re) and Richardson number (Ri) on the horizontal and vertical velocity components at the enclosure-mid section. It is clear that the horizontal and vertical velocity components depends strongly on the studied parameters and its variation affect the streamlines pattern. The vertical velocity component (V) vary with (Y) and approach its maximum value at nearly the mid-point of the upper half of the enclosure leading to lift and condense the streamlines at the upper half and that is reveals clearly from the dense concentration of the streamlines at that part as shown in figures (2, 4, 6 & 8). In addition, increase in both Ha and Re (at Ha=10) lead to decrease in the vertical velocity component (V) due to the dominating effect of Hartmann number (Ha). The results also show that the vertical velocity component increases with increasing values of J and Ri. The horizontal velocity component (U) show the same trend of variation as above at the lower part of the enclosure but there is a reverse trend of variation with (Y) starts nearly at (Y=0.6) where the main vortex exist, except that for the effect of Ri as it occur at nearly (Y=0.7) due to the effect of buoyancy force. At (Ri=0.), the values of (U&V≈0) are nearly zero at the mid section of the enclosure and that leads to fix the position of the main vortex as shown in figure (8-a).

6- Conclusions:

In the present numerical study the effect of magnetic parameter Hartmann number (Ha), Joule heating parameter (J), Richardson number (Ri) and Reynolds number (Re) on mixed convection flow in a vertical lid-driven square enclosure with a heat conducting horizontal semi circular cylinders has been performed. From the present investigations we may conclude that the heat transfer and the flow characteristics depend strongly upon the strength of the magnetic field. A significant effect of Hartmann number on the stream lines and isotherms is observed. The overall heat transfer decreases with the increasing of (Ha) and the lowest average temperature in the enclosure is found for Ha=40.0.

A little effect of the joule heating parameter (J) on the stream lines is observed, but significant effect on isotherms is noticed. The overall heat transfer decreases with the increase of (J) and the lowest average temperature in the enclosure is found for J=0.0.

Reynolds number strongly affects the stream lines and isotherms patterns. Higher heat transfer rates is observed for large Reynolds number, and average temperature in the enclosure become also higher with increment of (Re).

Buoyancy effect parameter (Ri) significantly affects the flow structure and heat transfer rates inside the enclosure.

The horizontal and vertical velocity components strongly affected by the above mentioned parameters and its variation affect the streamlines pattern and vortex position.

The result of the present work for the particular case (of changing average Nusselt number with Ha) at a specified boundary conditions is in excellent agreement with those of the already published work by ref. [5] at the same boundary conditions.

Nomenclature:

B_o	Magnetic induction (Wb/m^2).	C_p	Specific heat at constant pressure ($kJ/kg.^oK$).
c,h ,s	Subscripts denotes cold, hot and solid.	D	Dimensionless diameter of the semi cylinder.
g	Gravitational acceleration, (m/s^2).	Gr	Grashof number ($g\beta_e(T_h-T_c)\ H^3/\nu^2$).
Ha	Hartmann number.	h	Convection heat transfer coefficient ($W/m^2.^oK$).
J	Joule heating parameter.	K	Solid fluid thermal conductivity ratio.
k_f	Thermal conductivity of fluid ($W/m.^oK$).	k_s	Thermal conductivity of semi cylinder ($W/m.^oK$).
L	Enclosure length.(m)	Nu	Nusselt number.
P	Dimensionless pressure.	Pr	Prandtl number (ν/α_e).
Re	Reynolds number (U_oH/ν).	Ri	Richardson number (Gr/Re^2).
U, V	Dimensionless velocities in X &Y-directions.	U_o	Dimensionless lid velocity.
u,v	Velocities in x & y-directions, (m/s).	$\bar{V}$	Enclosure volume (m^3).
x,y	Cartesian coordinates.	X,Y	Dimensionless Cartesian coordinates.
α	Effective thermal diffusivity of fluid. (m^2/s).	β	Coefficient of thermal expansion of fluid (K^{-1}).
ν,μ	Kinematic and dynamic viscosity of fluid (m^2/s).	ρ	Fluid density (kg/m^3).
θ	Dimensionless temperature $[(T-T_c)/(T_h-T_c)]$.	σ	Fluid electrical thermal conductivity ($\Omega^{-1}m^{-1}$).

Appendix A

The name iso-parametric derives from the fact that the same parametric function describing the geometry may be used for interpolating spatial variable within an element. Fig. 1b shows an element with non-uniform shape mapped to a square one. The transformations between (X,Y) and (ζ,η) coordinates were defined by equation (16). The nine basis functions are:

$\Phi_1=(1-3\zeta+2\zeta^2)(1-3\eta+2\eta^2)$
$\Phi_2=(1-3\zeta+2\zeta^2)(4\eta-4\eta^2)$
$\Phi_3=(1-3\zeta+2\zeta^2)(-\eta+2\eta^2)$
$\Phi_4=(-\zeta+2\zeta^2)(1-3\eta+2\eta^2)$
$\Phi_5=(-\zeta+2\zeta^2)(4\eta-4\eta^2)$
$\Phi_6=(-\zeta+2\zeta^2)(-\eta+2\eta^2)$
$\Phi_7=(4\zeta-4\zeta^2)(1-3\eta+2\eta^2)$
$\Phi_8=(4\zeta-4\zeta^2)(4\eta-4\eta^2)$
$\Phi_9=(4\zeta-4\zeta^2)(-\eta+2\eta^2)$

The above basis functions are used for mapping the non-uniform domain or elements within the domain into square domain and also used for the evaluation of the integrals of residuals.

References:

1. Garandet, J.P., Alboussiere, T., Moreau, R. "Buoyancy driven convection in a rectangular enclosure with a transverse magnetic field", *International Journal of Heat and Mass Transfer*, Vol. 35, pp.741-748, 1992.
2. Rudraiah, N., Venkatachalappa, M., and Subbaraya, C.K., "Combined surface tension and buoyancy-driven convection in a rectangular open cavity in the presence of magnetic field.", *International Journal of Non-Linear Mechanics*, Vol. 30, pp.759-770, 1995.
3. Rudraiah, N., Barron, R.M., Venkatachalappa, M., and Subbaraya, C.K., "Effect of a magnetic field on free convection in a rectangular enclosure.", *International Journal of Engineering Science*, Vol. 33, pp.1075-1084, 1995.
4. Khanafer, K.M. and Chamkha, A.J. "Mixed convection flow in a lid driven enclosure filled with a fluid-saturated porous medium", *Int. J. Heat Mass transfer*, Vol.42, pp.2465-2481, 1999.
5. Chamkha,A.J."Hydro-magnetic combined convection flow in a vertical lid-driven cavity with internal heat generation or absorption",*Numerical Heat Transfer,Part A*,Vol.41, pp.529-546, 2003.
6. Kakarantzas, S. C., Sarris, I. E., Grecos, A. P. and Vlachos, N. S., "Magneto-hydrodynamic natural convection in a vertical cylindrical cavity with sinusoidal upper wall temperature", *Int. J.of Heat and Mass transfer*, Vol.52,No.(1-2) pp.250-259, 2009.
7. Rahman, M. M., Mamun, M.A.H., Saidur, R., Nagata, S. "Effect of a heat conducting horizontal circular cylinder on MHD mixed convection in lid-driven cavity along with joule heating", *Int. J. of Mechanical and Materials Engineering*, Vol. 4(3), pp.256-265, 2009.
8. Rahman, M. M., Alim, M. A., Sarker, M.M.A., "Numerical study on the conjugate effect of joule heating and magnato-hydrodynamics mixed convection in an obstructed lid-driven square cavity", *Int. Commun.Heat and Mass Transfer*, 37(5), pp.524-534, 2010.
9. Sivasankaran, S., Malleswaran, A., Lee, J., Sundar, P., "Hydro-magnetic combined convection in a lid-driven cavity with sinusoidal boundary conditions on both side walls", *Int. J. Heat Mass Transfer*, Vol. 54, pp.512-525, 2011.
10. Billah M.M., Rahman M.M., Saidur R. and hassnuzzaman M. "Simulation of MHD mixed convection heat transfer enhanced in a double lid-driven obstructed enclosure", *Int. J. of Mechanical and Materials Engineering (IJMME)*, Vol. 6, No.1, pp.18-30, 2011.
11. Tinsley Oden J., Noboru Kikuchi and Young Joon Song "Penalty-Finite Element methods for the analysis of Stokesian flows", *Computer Methods In Applied Mechanics and Engineering*, Vol.31, pp.297-329, (1982), NORTH HOLLAND PUBLISHING COMPANY.
12. R. Eid "Higher order isoparametric finite element solution of stokes flow", *Applied Mathematics and computation*, Vol. 162, pp.1083-1101, 2005.
13. J.N. Reddy "An introduction to the finite element method", *McGraw Hill New York, 1993.*

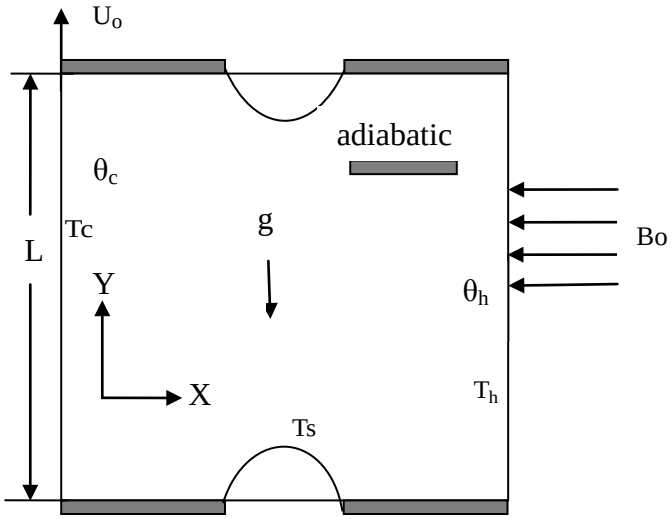

Fig.(1a): Schematic diagram of the physical model.

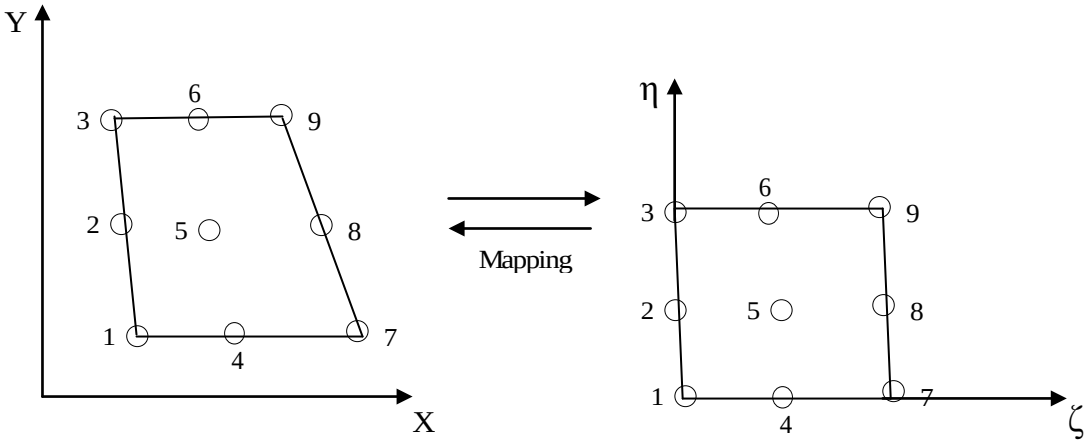

Global co-ordinate system Local co-ordinate system

Fig.(1b): The mapping of an individual element to a single element in (ζ-η) coordinate system.

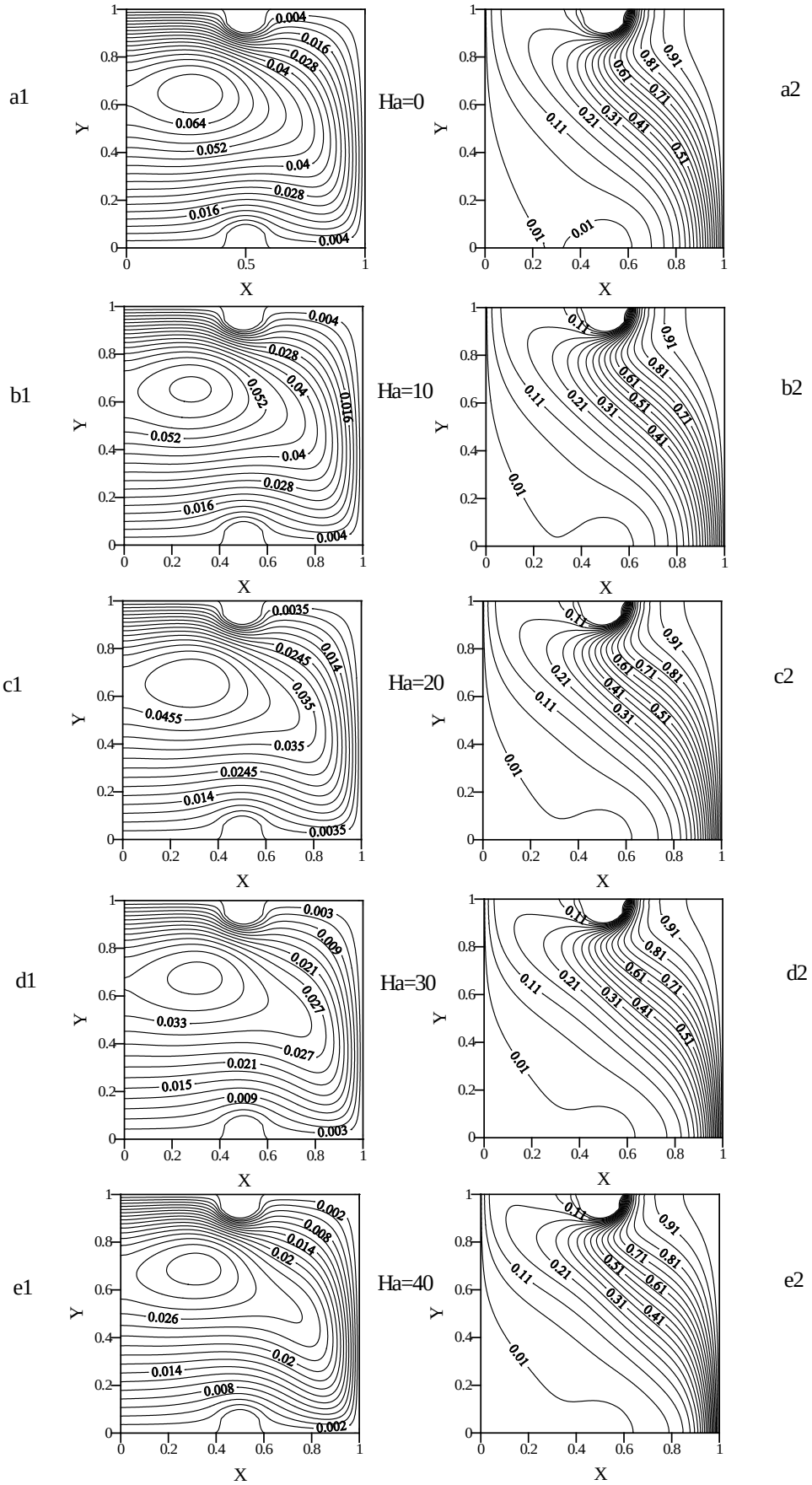

.Fig.(2): Streamlines on the left and isotherms on the right for (Ha=0,10,20,30 & 40) while Ri=1.0, Pr=0.71, Re=100 and J=1.0.

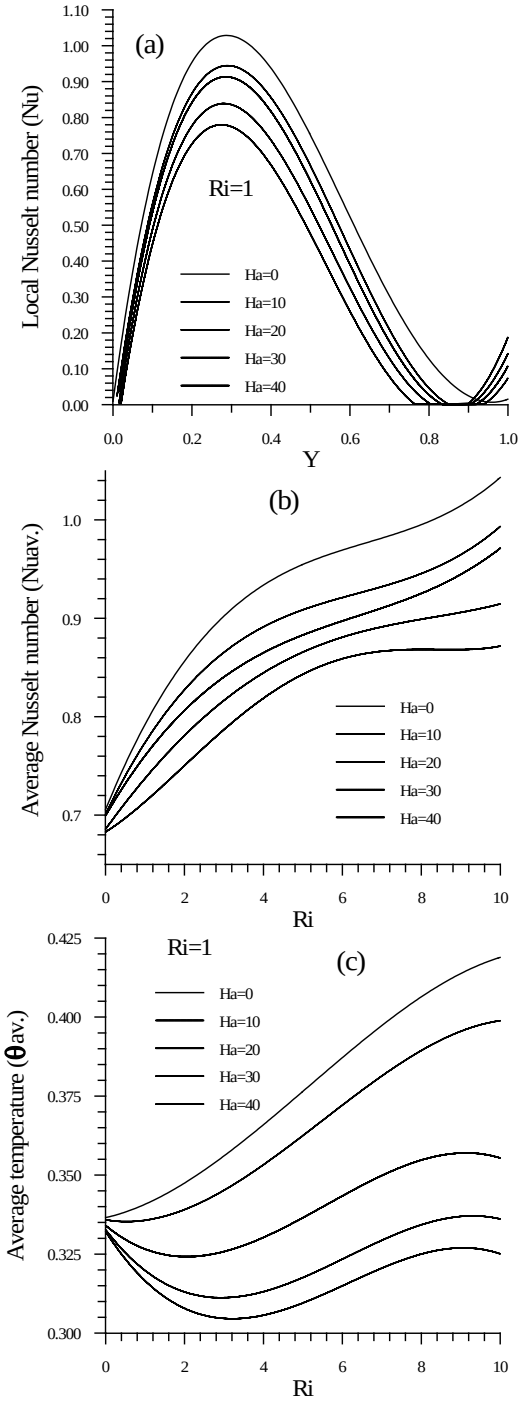

Fig. (3) : The effect of Hartmann number (Ha) on local, average Nusselt number and average temperature at Pr=0.71, Re=100 & J=1.0.

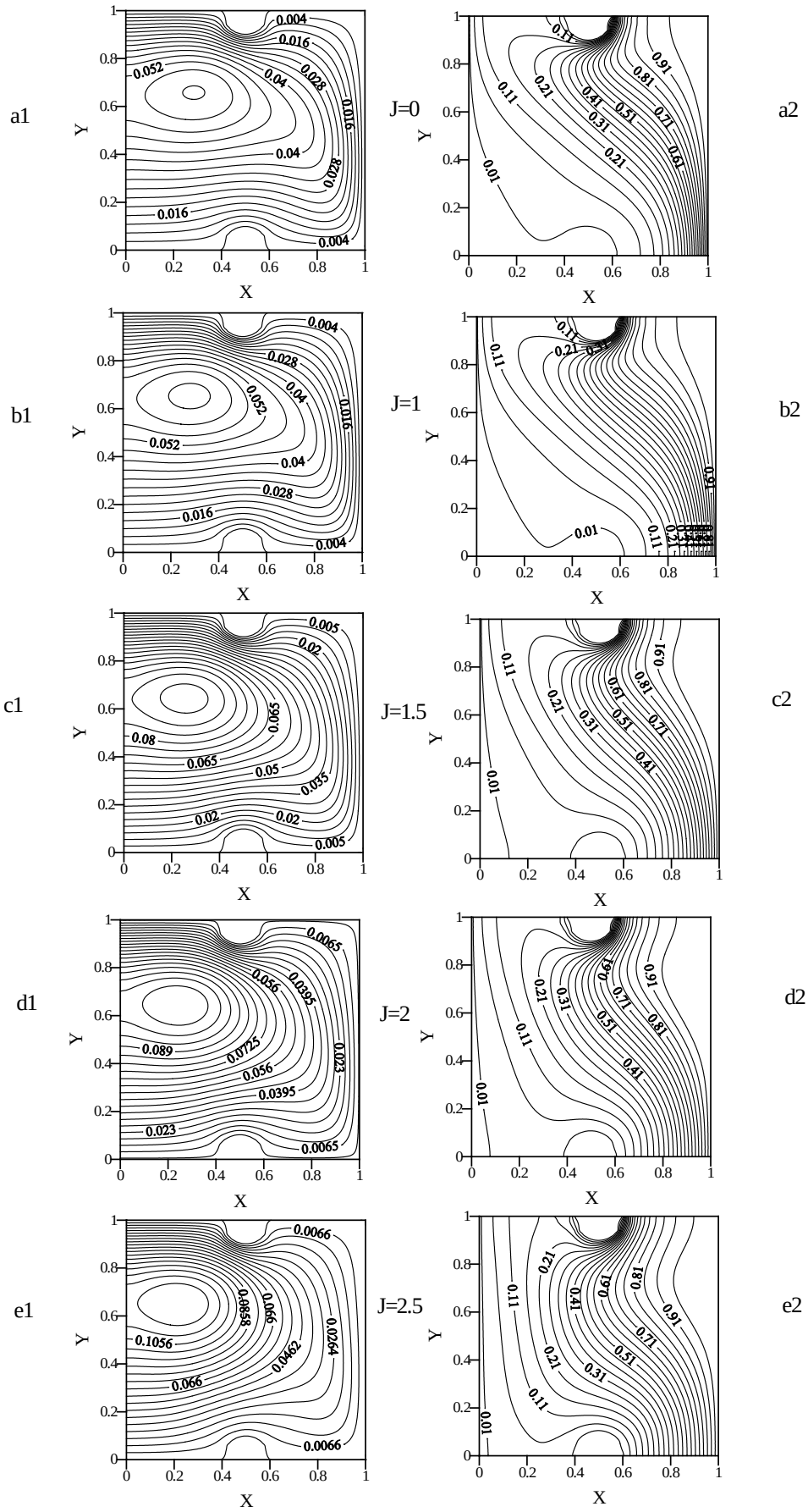

.Fig.(4): Streamlines on the left and isotherms on the right for (J=0,1,1.5, 2 & 2.5) while Ri=1.0, Pr=0.71, Re=100 and Ha=10.

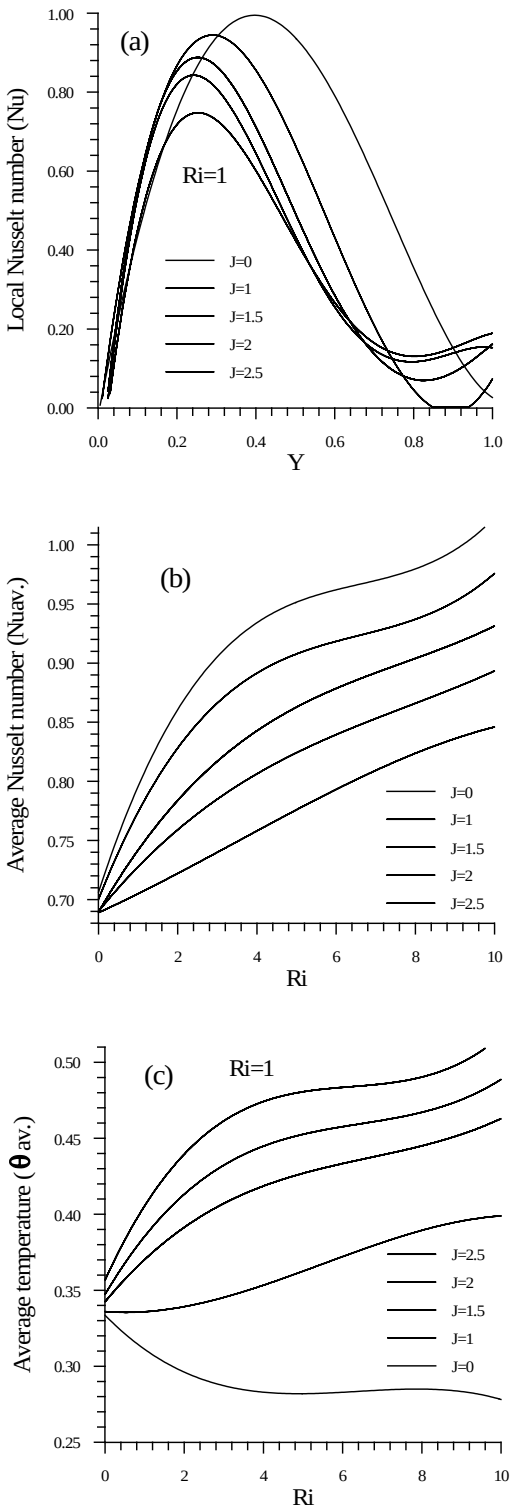

Fig. (5) : The effect of Joule heating parameter (J) on local, average Nusselt number and average temperature at Pr=0.71, Re=100 & Ha=10.

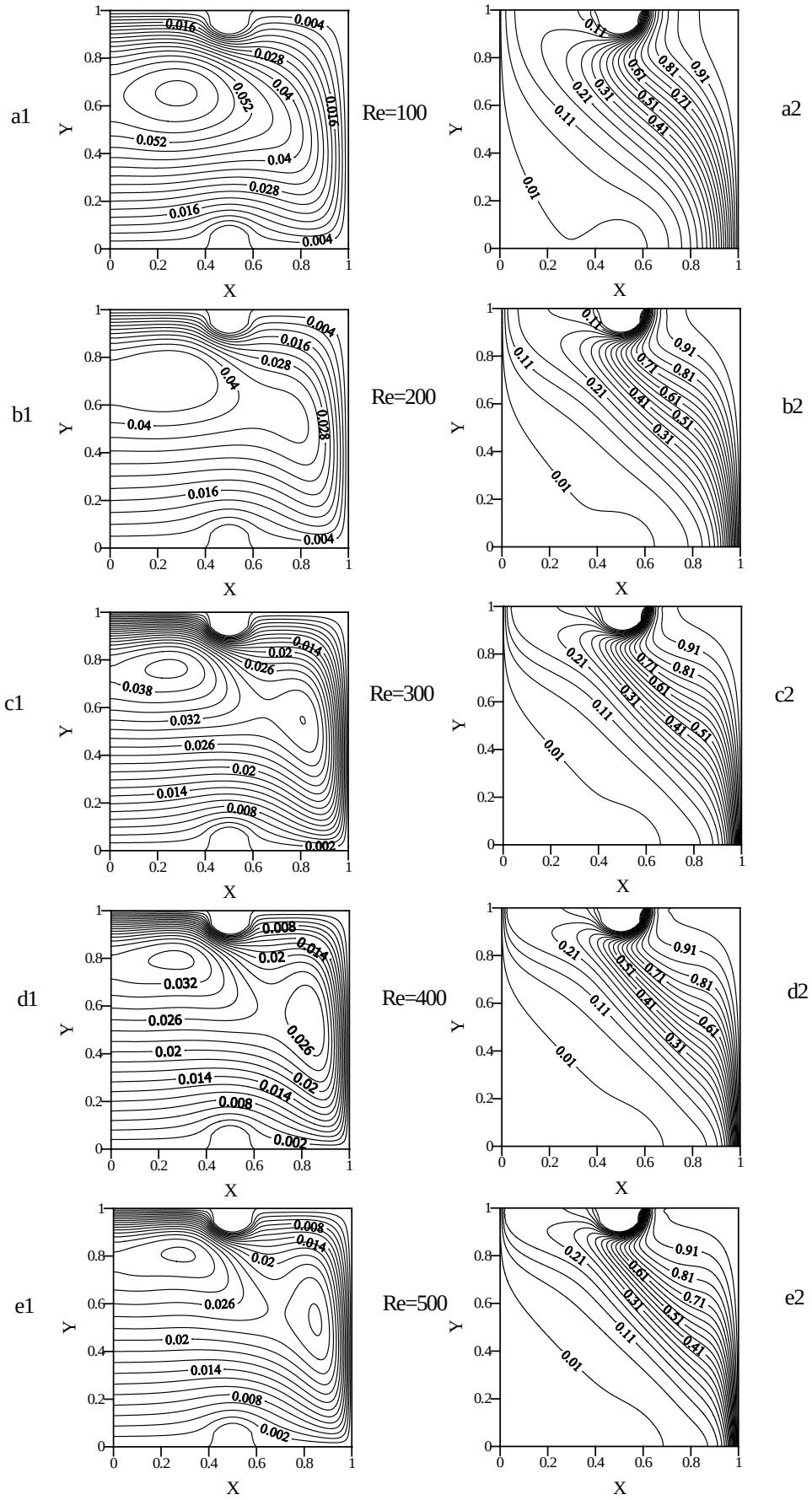

.Fig.(6): Streamlines on the left and isotherms on the right for (Re=100,200,300,400 & 500) while Pr=0.71, Ri=1.0 , J=1.0, and Ha=10.

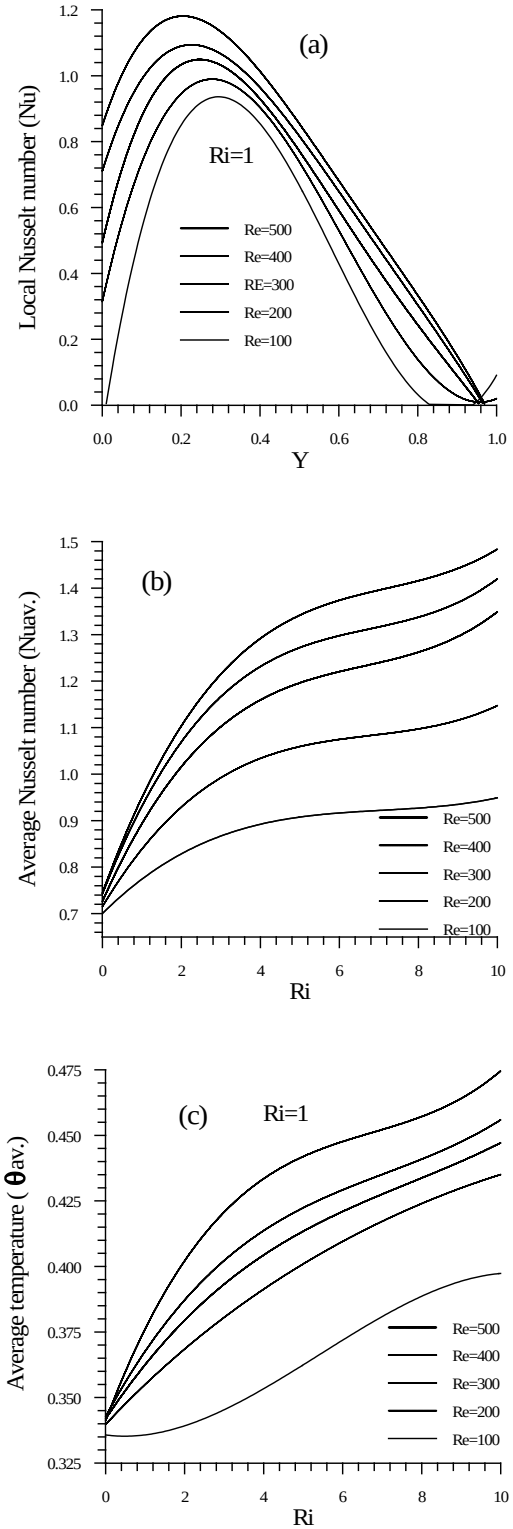

Fig. (7) : The effect of Reynolds number on local, average Nusselt number and average temperature at Pr=0.71, Ha=10 & J=1.0.

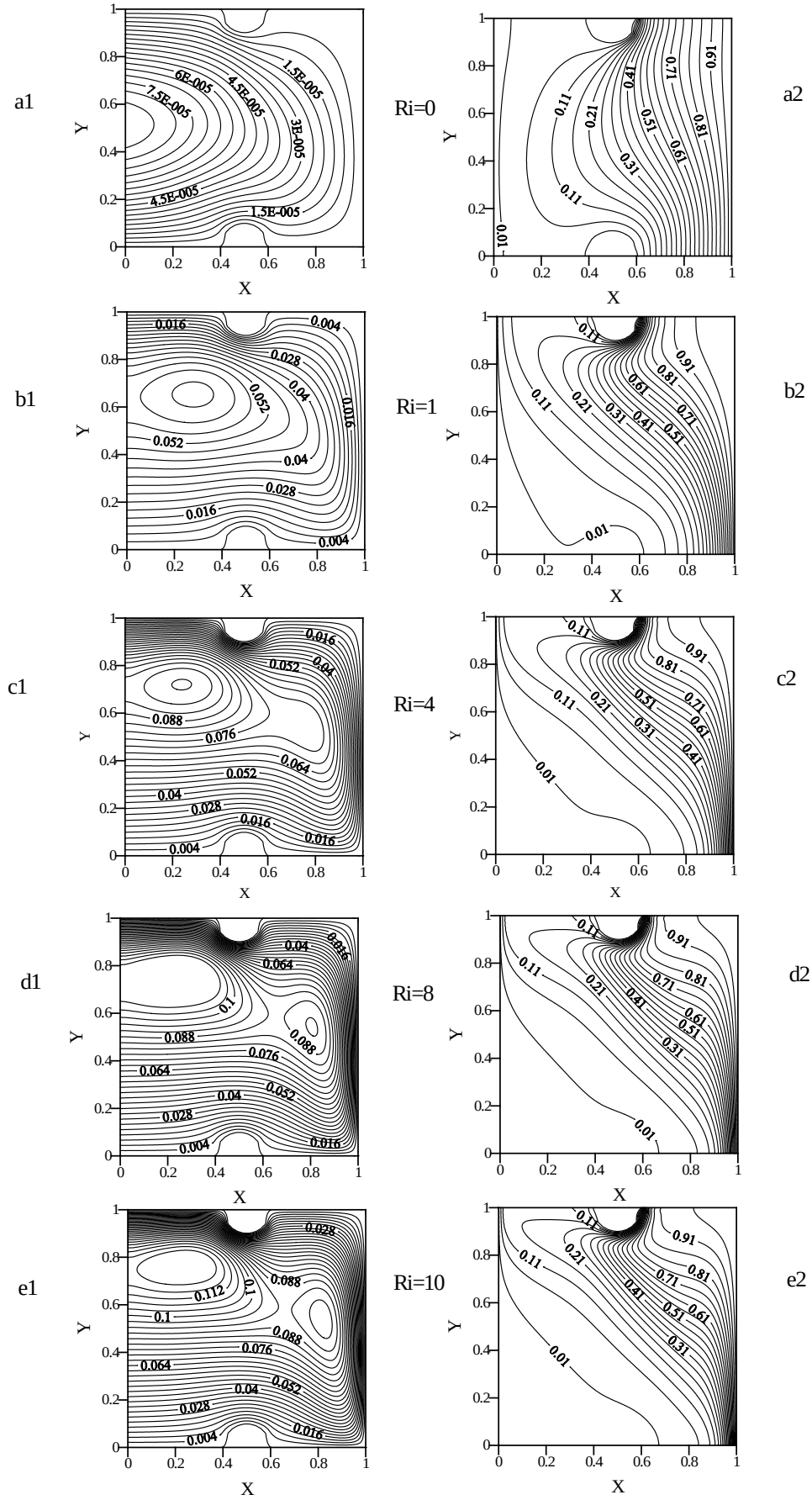

.Fig.(8): Streamlines on the left and isotherms on the right for (Ri=0, 1, 4, 8 & 10) while Pr=0.71, Re=100 , J=1.0, and Ha=10.

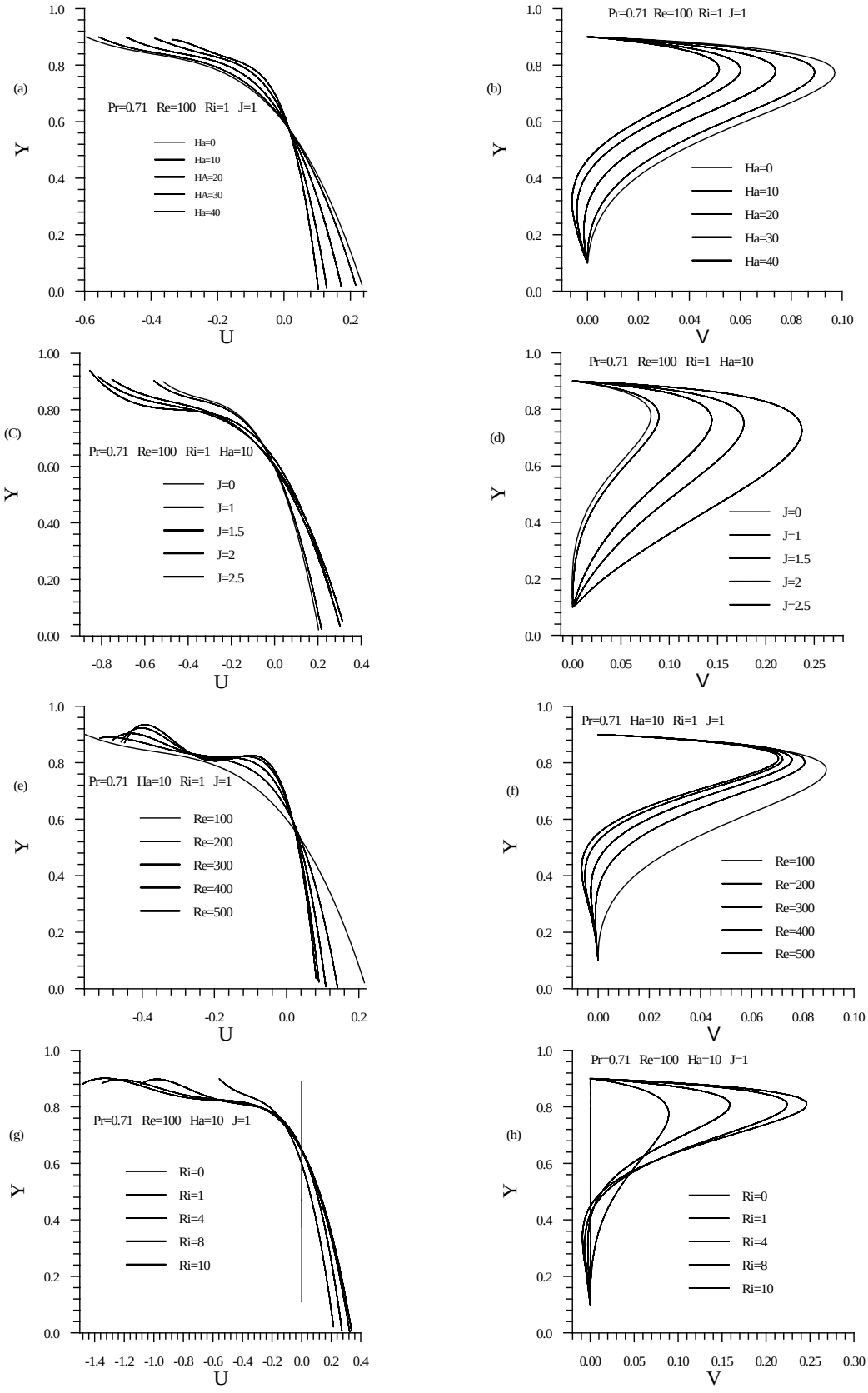

Figure (9): Horizontal and Vertical velocity components at the enclosure mid section (X=0.5) for different values of dimensionless parameters.